



Changes in soil pore structure generated by the root systems of maize, sorghum and switchgrass affect in situ N_2O emissions and bacterial denitrification

Maik Lucas^{1,2} · J. Gil^{3,4} · G. P. Robertson^{1,5} · N. E. Ostrom³ · A. Kravchenko¹

Received: 13 April 2023 / Revised: 27 July 2023 / Accepted: 28 July 2023
© The Author(s) 2023

Abstract

Due to the heterogeneous nature of soil pore structure, processes such as nitrification and denitrification can occur simultaneously at microscopic levels, making prediction of small-scale nitrous oxide (N_2O) emissions in the field notoriously difficult. We assessed $\text{N}_2\text{O}+\text{N}_2$ emissions from soils under maize (*Zea mays* L.), switchgrass (*Panicum virgatum* L.), and energy sorghum (*Sorghum bicolor* L.), three potential bioenergy crops in order to identify the importance of different N_2O sources to microsite production, and relate N_2O source differences to crop-associated differences in pore structure formation. The combination of isotopic surveys of N_2O in the field during one growing season and X-ray computed tomography (CT) enabled us to link results from isotopic mappings to soil structural properties. Further, our methodology allowed us to evaluate the potential for in situ N_2O suppression by biological nitrification inhibition (BNI) in energy sorghum. Our results demonstrated that the fraction of N_2O originating from bacterial denitrification and reduction of N_2O to N_2 is largely determined by the volume of particulate organic matter occluded within the soil matrix and the anaerobic soil volume. Bacterial denitrification was greater in switchgrass than in the annual crops, related to changes in pore structure caused by the coarse root system. This led to high N-loses through N_2 emissions in the switchgrass system throughout the season a novel finding given the lack of data in the literature for total denitrification. Isotopic mapping indicated no differences in N_2O -fluxes or their source processes between maize and energy sorghum that could be associated with the release of BNI by the investigated sorghum variety. The results of this research show how differences in soil pore structures among cropping systems can determine both N_2O production via denitrification and total denitrification N losses in situ.

Keywords Nitrification · N_2O isotope mapping · X-ray CT · Anaerobic soil volume · Plant roots · Pore structure · BNI

Introduction

N_2O is a highly potent greenhouse gas with a substantial global warming impact that can also harm the stratospheric ozone layer (Ravishankara et al. 2009; Tian et al. 2020). Agriculture is responsible for the majority (60%) of anthropogenic N_2O emissions (Syakila and Kroeze 2011), through management practices like tillage and fertilizer application (Butterbach-Bahl and Dannenmann 2011; McGill et al. 2018; McSwiney and Robertson 2005). Biofuels from cellulosic bioenergy feedstocks make it possible to reduce the climate impact of fossil fuel energy consumption; their positive contribution to mitigating climate change, however, might be diminished by greenhouse gas (GHG) emissions, including N_2O (Oates et al. 2016; Qin et al. 2015; Walter et al. 2015; Wightman et al. 2015). While N_2O production is known to be affected by plant species composition (Butterbach-Bahl

✉ Maik Lucas
maik.lucas@ufz.de

¹ DOE Great Lakes Bioenergy Research Center and Department of Plant, Soil and Microbial Sciences, Michigan State University, East Lansing, MI, USA

² Department of Soil System Sciences, Helmholtz Centre for Environmental Research, Halle, Germany

³ Department of Integrative Biology, Great Lakes Bioenergy Research Center, Michigan State University, East Lansing, MI 48824, USA

⁴ Department of Environmental and Biological Sciences, University of Eastern Finland, Kuopio, Finland

⁵ W.K. Kellogg Biological Station, Michigan State University, Hickory Corners, MI 49060, USA

and Dannenmann 2011; Stehfest and Bouwman 2006) we do not fully understand the mechanisms influencing N_2O emission from soils under different vegetation systems well enough to develop effective solutions for curbing overall GHG emissions.

In soils, N_2O is a product of an array of N transformations (Robertson and Groffman 2015), with heterotrophic bacterial denitrification (bD), autotrophic nitrification (Ni), nitrifier denitrification (nD), and fungal denitrification (fD) regarded as primary sources (Butterbach-Bahl et al. 2013; Müller et al. 2014). Even though these processes may drastically differ from each other in terms of conditions necessary for their occurrence and the microorganisms involved, the extremely high micro-scale heterogeneity of the soil matrix enables them to produce N_2O in a close spatial proximity (Braker and Conrad 2011; Rohe et al. 2021). Disentangling the specific drivers responsible for enhanced N_2O emissions in the field is therefore notoriously difficult.

Availability of O_2 is one of the major physical factors controlling N_2O fluxes (Bollmann and Conrad 1998; Groffman et al. 1988; Rohe et al. 2021). For example, O_2 discriminates between N_2O production via denitrification, i.e. the anoxic reduction of nitrate (NO_3^-) to N_2 with N_2O as an intermediate, which takes place in the absence of O_2 , and nitrification, where N_2O is a by-product during the oxidation of hydroxylamine (NH_2OH) to nitrite (NO_2^-), which requires aerobic conditions. In contrast to bD, the major end product of fD is N_2O since fungal denitrifiers lack N_2O reductase (Baggs 2011; Philippot et al. 2011). In contrast to coupled nitrification-denitrification where the formation of nitrate and subsequent nitrate reduction are conducted by different microorganisms, in nD these tasks are performed by the same organism, the process benefitting from low organic C and O_2 but high N availability (Braker and Conrad 2011; Wrage et al. 2001).

Denitrification is thus favored by wet conditions, available C and nitrate, and is often a major N_2O source during high N_2O flux events (Baggs 2011; Wrage et al. 2004). Yet, denitrification also can make surprisingly sizeable contributions to N_2O fluxes from relatively dry soils. The latter is an outcome of local anaerobicity observed within decomposing plant residues or within soil matrix, e.g., centers of soil aggregates (Schlüter et al. 2018; Wrage et al. 2001). Occurrence and proliferation of anaerobic microsites within the soil matrix, which we will refer to as anaerobic soil volume fraction, is hard to quantify directly, but can be assessed indirectly through measures of diffusivity as well as model simulations based on air-filled pore volumes (Andersen and Petersen 2009; Balaine et al. 2013). Anaerobic soil volume fraction can also be manipulated in bulk (whole) soil samples by controlling the water filled pore space (WFPS) (Chen et al. 2016; Kim et al. 2022; Kravchenko et al. 2017). The WFPS 70–80% has been shown to be optimal for denitrification (Butterbach-Bahl

et al. 2013). However, such bulk measurements do not consider pore structure, a key factor controlling the microscale distribution patterns in anaerobic soil volume fraction. Recent advancements in X-ray computed tomography (X-ray CT) imaging allowed visualization of anaerobic soil volume fraction at micro-scales and demonstrated that anaerobic soil volume fraction, quantified via distances to air-filled pores, can predict N_2O emissions as well as magnitudes of complete denitrification (Kravchenko et al. 2018; Rabot et al. 2015; Rohe et al. 2021).

Not only O_2 influx, but also O_2 demand is highly controlled by the pore architecture. Intense microbial activity boosts oxygen consumption, creating local anaerobic microsites which stimulates N_2O production (Kim et al. 2020, 2021; Kravchenko et al. 2017). Microbial activity's impact on N_2O emissions thus depends on pore architecture in a complex not yet fully understood manner. Some studies suggest that narrow macropores (30–150 μm diameter (\emptyset)) can provide a perfect environment for microbial decomposers, hence, for close spatial coupling of N_2O production and emission during decomposition of fresh plant residues (Kim et al. 2020, 2021, 2022; Kravchenko et al. 2017). Yet, lower availability of O_2 stimulated by greater distances from pores to decomposing soil particulate organic matter (POM) can enhance N_2O emissions (Ortega-Ramírez et al. 2023).

Plant roots play the most important role in shaping soil pore architecture through direct formation of biopores and indirect repacking and rearranging of soil solids (Lucas et al. 2019, 2022). Biopores formed by roots range from ~30 μm to 5000 μm , i.e. span three orders of magnitude (Yunusa and Newton 2003). Narrow biopores (e.g., 30–150 μm \emptyset) can be particularly important due to their oversize contribution to the overall connectivity of the pore system (Lucas et al. 2020). Differences in root architectures in plants of different species or plant communities can have a sizeable influence on narrow macropore formation (Bacq-Labreuil et al. 2019; Bodner et al. 2014; Lucas et al. 2022), hence potentially influencing the size of anaerobic soil volume fraction. For example, a comparison of several bioenergy cropping systems demonstrated that polyculture vegetation communities decreased soil anaerobic soil volume fraction compared to monoculture maize and switchgrass, and that such decreases were associated with lower N_2O emissions (Kravchenko et al. 2018).

The other two important routes through which roots can affect N_2O emissions are through direct alterations of soil N balance through N uptake vs. N inputs via exudation and rhizodeposition (Jones et al. 2009; Moreau et al. 2019), and by shaping the composition and functions of the soil microbiome and rhizosphere processes (Berendsen et al. 2012; Hinsinger et al. 2009). However, the actual significance of plant-microbe interactions for the soil N-cycle, e.g. through the release of labile C as drivers of rhizosphere

denitrification, is currently not well understood (Baggs 2011; Moreau et al. 2019; Philippot et al. 2009). Certain plant species, e.g., sorghum a promising bioenergy crop, can produce and release biological nitrification inhibitors (BNIs) into the soil, potentially suppressing nitrification, through the reduction of ammonia-oxidizing bacteria and archaea (Li et al. 2021; Sarr et al. 2020; Subbarao et al. 2007, 2015; Tesfamariam et al. 2014). However, sizes and ecological impacts of biological nitrification inhibition of sorghum in the field are yet to be determined by measurements of in-situ gross nitrification and denitrification, such as through isotopic techniques (Nardi et al. 2022).

With few exceptions, for example, Rohe et al. (2021), previous studies measured only the emitted N_2O , lacking the ability to identify the processes that led to its production or to assess the full extent of denitrification. Therefore, while N losses in the soil in the form of N_2 can be substantial, their measurements are complicated by a high atmospheric N_2 background (Lewicka-Szczebak et al. 2017; Yu et al. 2020). By analyzing the isotopic signatures of N_2O , including the $\delta^{18}\text{O}$ value of oxygen, the bulk $\delta^{15}\text{N}$ value, and the intra-molecular distribution of ^{15}N in N_2O (site preference, SP), it is possible to gain insights into the origins of N_2O emissions (Yu et al. 2020). A way to derive quantitative information on N_2O sources from such isotopic analyses is isotopic mapping using $\delta^{15}\text{N}^{\text{SP}} / \delta^{18}\text{O}$ (Yu et al. 2020). Based on the isotopic enrichment of residual N_2O during the reduction to N_2 , it further allows to derive denitrification product ratio [$\text{N}_2\text{O} / (\text{N}_2\text{O} + \text{N}_2)$] (pr) and thus to quantify complete denitrification through $\text{N}_2\text{O} + \text{N}_2$ fluxes (Lewicka-Szczebak et al. 2017).

The objectives of the study were 1) to conduct field monitoring of N_2O and comparisons of $\text{N}_2\text{O} + \text{N}_2$ emissions and their N_2O component from the soils under energy sorghum, maize and switchgrass crops, grown for bioenergy stock production; 2) to distinguish among the prevalent pathways of N_2O production in the soils of these crops; and 3) to elucidate the potential role of soil pore structure for influencing $\text{N}_2\text{O} + \text{N}_2$ emissions and their sources. We collected N_2O throughout the growing season using static flux chambers and implemented $\delta^{15}\text{N}^{\text{SP}} / \delta^{18}\text{O}$ isotope mapping to estimate the relative contribution of different microbial pathways to N_2O production as well as to quantify the reduction of N_2O to N_2 . X-ray CT imaging of undisturbed soil cores allowed us to quantify pore structure and elucidate its contribution to micro-environmental conditions prevalent within the soil matrix. We also hypothesized that the reported ability of sorghum roots, in contrast to maize, to reduce nitrification potential by BNI (Subbarao et al. 2007; Tesfamariam et al. 2014) will be manifested in the field through greater N_2O production via denitrification than nitrification pathway. We also hypothesized that a capacity of switchgrass to reduce narrow macropores and increase the anaerobic soil volume

(Kravchenko et al. 2019, 2022) will result in an increased importance of complete denitrification, as compared to that in the other two crops.

Methods

Field design and management

The DOE-Great Lakes Bioenergy Research Center (GLBRC) Biofuel Cropping System Experiment (BCSE) site was established in 2008 at the Kellogg Biological Station (KBS) Long-term Ecological Research site (Robertson and Hamilton 2015) in Hickory Corners, Michigan [$42^{\circ}23'47''$ N, $-85^{\circ}22'26''$ W, 288 m a.s.l.]. Site soils are loamy, well-drained Alfisols developed on glacial outwash with loess inputs. The experiment is a randomized complete block design with five replicate blocks. We evaluated N_2O emissions from three systems during the 2021 field season: Monocultures of switchgrass (*P. virgatum* L. variety Cave-in-rock), maize (*Zea mays* L., Pioneer P0306Q) and energy sorghum (*Sorghum bicolor* L., TAM 17651). Before 2018, the energy sorghum plots contained continuous maize + cover crops.

Seeding and fertilizer application differed between the treatments (Fig. 2a, top row). Details on the agricultural management in 2021 and before can be found on <https://aglog.kbs.msu.edu/>. In summary, maize was seeded on the 15th of May with a starter fertilizer supplying 34 kg N ha⁻¹ and energy sorghum was seeded on the 19th of May with 56 kg N ha⁻¹. At the end of June an additional 137 kg N ha⁻¹ (28% Urea Ammonium Nitrate, UAN) was injected in the middle of the rows of the two crops. The switchgrass plots were sprayed with 28% UAN on the 13th of May supplying 56 kg N ha⁻¹ with no further N additions. All systems were managed without tillage.

N_2O sampling

Two static (closed-cover) flux chambers were installed within 2 m of one another in each of the five blocks in May 2021 and removed only for agronomic operations for a total of 10 chambers per cropping system. Each chamber consisted of a cylindrical metal base and an airtight plastic lid (surface area = 641 cm², headspace volume = 16.6 L) and was hammered 5 cm deep in the soil. Atmospheric pressure within the sealed chamber was maintained by a piece of coiled stainless-steel tubing (0.5 m X 0.32 cm OD and 0.18 cm ID) extending from the interior to exterior of the chamber. Gas samples were taken from an approx. 50 cm long and 0.6 mm outer diameter polyurethane tubing connected to the headspace (Fig. 1a). During sampling a pre-evacuated 250 ml glass bottle was connected to a steel needle at the

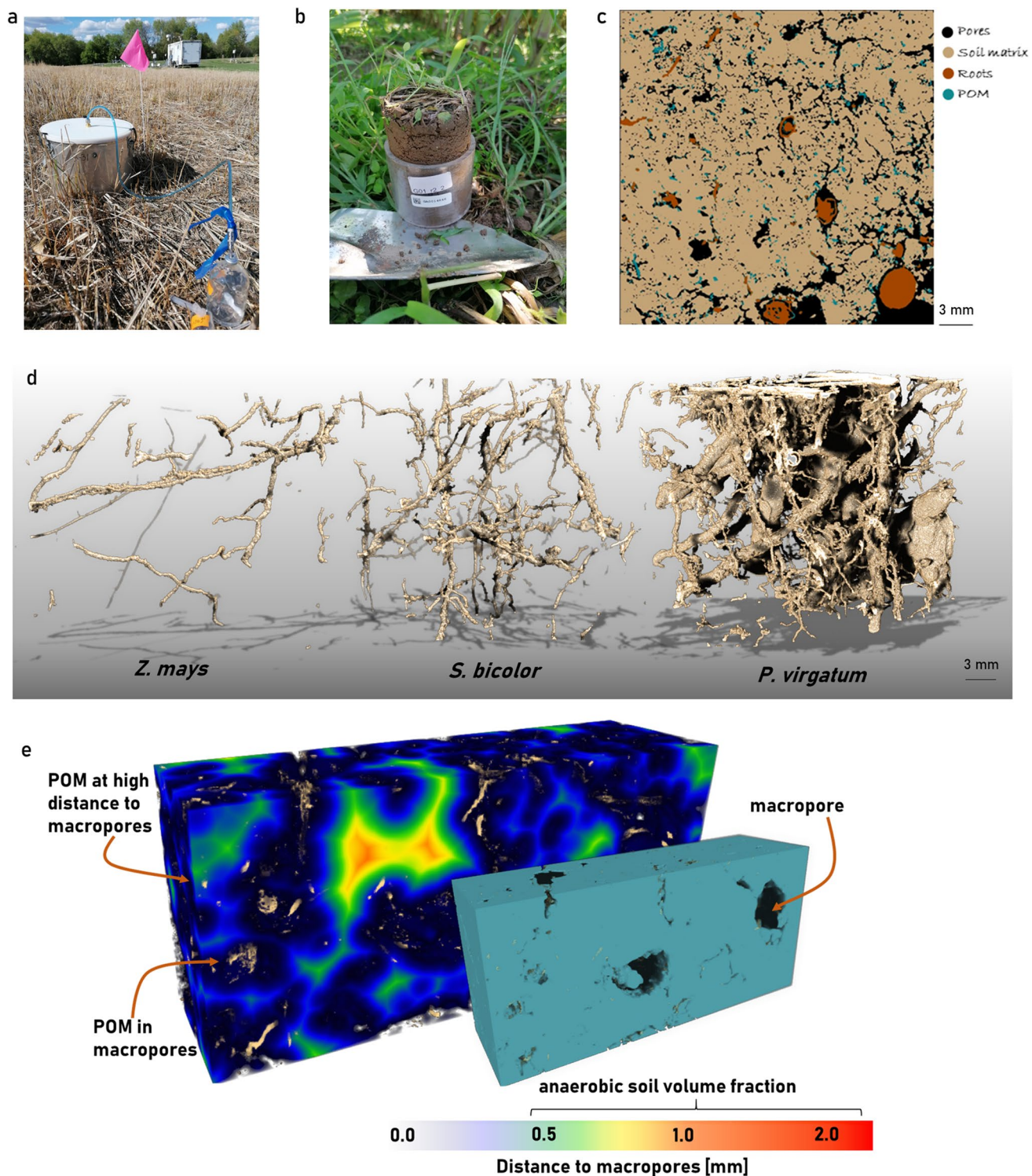
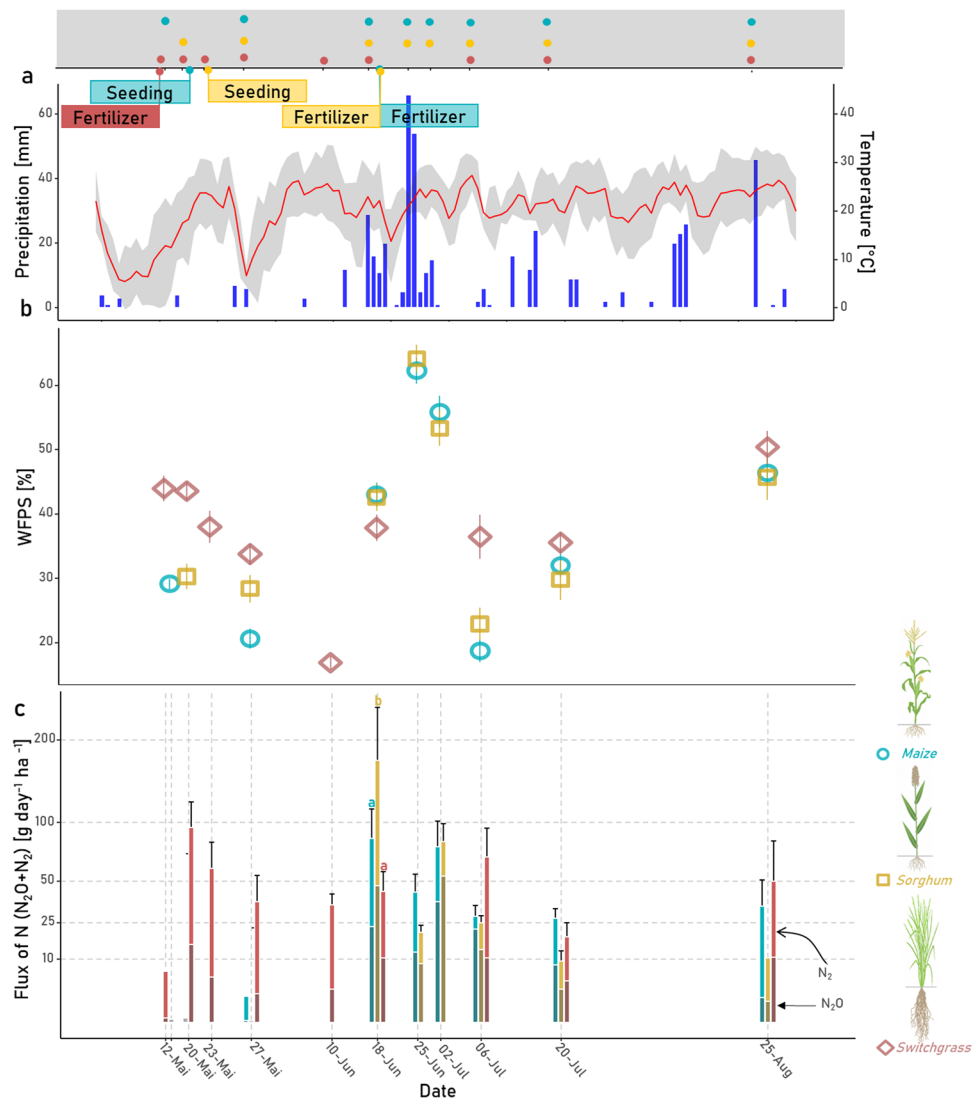


Fig. 1 Photographs and CT visualizations. **a)** Collecting N_2O from a static flux chamber at the beginning of the season. **b)** A soil core taken within the base of the chamber. **c)** An image slice from a CT-scanned soil core showing pores, roots, particulate organic matter (POM), and soil solid matrix identified on the image. **d)** Visualization

of the root system of maize, energy sorghum and switchgrass within the soil core obtained using X-ray CT and **e)** visualization of the soil matrix (turquoise) and macropores (black) as well as the visualization of POM (brown) within the 3D distance map to air-filled macropores.

Fig. 2 **a**) Daily precipitation (blue bars) and mean daily temperature (red line). Shadow represents max. and min temperature range. **b**) Water filled pore space (WFPS). **c**) $\text{N}_2\text{O}+\text{N}_2$ fluxes during the cropping season for the three bioenergy crops. The darkest parts of the bars represent the fraction of N_2O . The top row shows the sampling days for the three studied crops and marks the dates of seeding and fertilization events. Whiskers show the standard errors of the means. Different letters mark significant differences among the crops within the same sampling date ($p<0.05$). On some of the sampling dates N fluxes were too low to provide reliable isotopic values, thus no values are reported on **c**). Note that N_2 was calculated based on the pr derived from the isotopic mapping approach.



end of the tubing for 1 min to assure diffusive equilibration. Additionally, a 30 ml pre-evacuated glass bottle was filled. Chamber closing times ranged between 70 min and 470 min to ensure sufficient N_2O concentrations for later isotopic characterization. Initial closures were adjusted to the expected fluxes, i.e. with the shortest closing times for maize directly after fertilization and the longest for switchgrass before fertilization and timed to complete sampling by noon. Additionally, 250 ml atmospheric gas samples were taken on the respective sampling days in plot 1 of each of the respective plant treatments at the height of the top of the chamber.

Sampling was conducted throughout the 2021 season with 7–8 sampling events per crop. Some of the sampling events took place on a regular basis, i.e., once a month, throughout the growing season, with the first sampling on 12th of May and the last on 25th of August. Other sampling events targeted anticipated enhanced GHG emissions, including samplings at 3, 7, 14, and 30 days after N fertilization and

sampling on the day of the first large rain event (>30 mm, Fig. 2a) that followed a long May-June drought.

N_2O flux calculations

Measurements of N_2O concentration in the 30 ml samples were carried out using a gas chromatograph (GC-ECD, Shimadzu GC-2014) with an analytical precision of approx. 2%. Using these concentrations, the N_2O fluxes were calculated based on an increase in the N_2O concentration from that of air using the ambient mean of the measured N_2O concentration of 335 ppbv during the closing time. For all samples with N_2O concentrations > 300 ppbv, the paired taken 250 ml samples were used for isotopic characterization (see below). In that case, the N_2O concentration from respective analyses was used to calculate N_2O fluxes.

Isotopic characterisation

An Elementar IsoPrime 100 stable isotope ratio mass spectrometer (IRMS) interfaced to a Trace Gas inlet system (Elementar; Mt. Laurel, NJ) was used to measure $\delta^{15}\text{N}_{\text{bulk}}$, $\delta^{15}\text{N}_{\alpha}$, $\delta^{15}\text{N}_{\beta}$ and $\delta^{18}\text{O}$ of N_2O as previously described (Sutka et al. 2003). By analyzing the mass-to-charge (m/z) 44, 45, and 46 in intact N_2O^+ molecular ions, we determined the bulk $\delta^{15}\text{N}$ and $\delta^{18}\text{O}$ isotope signatures, while the $\delta^{15}\text{N}_{\alpha}$ values were detected by the m/z 30 and 31 of NO^+ fragment ions generated in the mass spectrometer. N_2O is a linear molecule consisting of two N atoms (NNO), with one of the N atoms in the central position (α site) and the other at the terminal position (β site). The distribution of ^{15}N within the N_2O molecule is called site preference (SP) and is defined as the difference in $\delta^{15}\text{N}$ values between the α ($\delta^{15}\text{N}_{\alpha}$) and β ($\delta^{15}\text{N}_{\beta}$) sites. The isotopic values are presented as deviation from the $^{15}\text{N}/^{14}\text{N}$ and $^{18}\text{O}/^{16}\text{O}$ ratios of atmospheric N_2 and the Vienna Standard Mean Ocean Water (VSMOW), respectively. The analytical precision determined as standard deviation (1σ) of primary standards measurements was 0.5‰ for $\delta^{15}\text{N}_{\text{bulk}}$ and $\delta^{18}\text{O}$, 0.4‰ for $\delta^{15}\text{N}_{\alpha}$, and $\delta^{15}\text{N}_{\beta}$ and 0.6‰ SP. The $\delta^{15}\text{N}_{\text{bulk}}$, $\delta^{15}\text{N}_{\alpha}$, $\delta^{15}\text{N}_{\beta}$, $\delta^{18}\text{O}$ and SP values of the two laboratory N_2O primary standards are -0.69‰, 11.51‰, -12.88‰, 40.16‰ and 24.39‰ and -0.77‰, -1.12‰, -0.42‰, 39.17‰ and -0.70‰, respectively as determined by calibration against international reference material USGS51 and USGS52 (Ostrom et al. 2018). The dilution of the ambient air in the flux chamber was corrected based on the increase in the N_2O concentration from that of the measured mean ambient concentration and the respective isotopic values throughout the season ($\delta^{15}\text{N}$ 6.1 ± 0.2 , $\delta^{15}\text{N}^{\text{SP}}$ 13.4 ± 0.5 , $\delta^{18}\text{O}$ 41.7 ± 0.2). To assure high accuracy, we further analyzed only isotopic readings of samples with N_2O concentrations greater than 130% of the ambient N_2O concentration.

We followed the " $\delta^{15}\text{N}^{\text{SP}} / \delta^{18}\text{O}$ isotope mapping technique" to estimate the relative contribution of the different microbial N_2O production pathways to the total $\text{N}_2\text{O} + \text{N}_2$ production (Lewicka-Szczebak et al. 2020; Yu et al. 2020). We used recently summarized data from Yu et al. (2020) to map the endmembers, i.e. the microbial source isotope values for bD/ nD and Ni processes and between bD/nD and fD as well as the N_2O reduction (Tab. S1). The $\delta^{18}\text{O}$ values were corrected for by the mean $\delta^{18}\text{O}$ of annual precipitation water (-7.3 ‰) derived from the Waterisotopes Database (<http://waterisotopesDB.org>). Accessed 01.11.2022). Adding the endmembers into the $\delta^{15}\text{N}^{\text{SP}} / \delta^{18}\text{O}$ isotope plot allows us to derive the different slopes of the mixing line between bD+nD and fD or Ni, as well as the reduction line for isotopic enrichment of residual N_2O . The latter allows us to calculate the denitrification product ratio [$\text{N}_2\text{O}/(\text{N}_2\text{O} + \text{N}_2)$] (pr) and

thus to derive total $\text{N}_2\text{O} + \text{N}_2$ emissions. Note that bD and nD cannot be distinguished by this method.

We followed a protocol (Lewicka-Szczebak et al. 2017, 2018) taking into account the sample position in the $\delta^{15}\text{N}^{\text{SP}} / \delta^{18}\text{O}$ map using a mixing equation for the bacterial fraction and the Rayleigh equation for N_2O reduction. In short, to derive the relative contributions of the endmembers, two scenarios are assumed, of which we present mean values: In the first, N_2O is produced by bD and partially reduced; then a mixing of residual N_2O with unreduced N_2O from Ni or fD appears. In the second, these processes happen vice versa. The $\delta^{18}\text{O}$ endmembers for Ni and fD taken from Yu et al. (2020) are sufficiently differentiated to allow both mixing-lines between bD-Ni and bD-fD to be distinguished (Lewicka-Szczebak et al. 2020). Since multiple mixing curves cannot be evaluated simultaneously with the equations of Lewicka-Szczebak (2018), we distinguished between bD-Ni and bD-fD mixing as two possible instances of end-member mixing as suggested in Lewicka-Szczebak et al. (2020). In the event that the samples were located below the mean reduction line, the calculation results provide the fraction of bD values slightly higher than 1, which were set to 1 for further summaries.

WFPS and N forms

Soil moisture was measured (0 – 10 cm depth) at three locations close to each chamber at every sampling event using a volumetric soil moisture sensor (HydroSense II, Campbell Scientific, Logan UT, USA).

Additionally, we took disturbed soil samples (~100g) from around the chambers at various time points throughout the season (Tab. S2), including sample dates before and after fertilization as well as after the rain event. The soil samples were stored at -20°C before extraction. For this, a homogenized sample of approx. 10 g of fresh soil was extracted with 0.1 mol KCl. Available NH_4^+ and NO_3^- were analyzed in the MSU soil test laboratory according to Sinsabaugh et al. (2000) and Doane and Horwáth (2003), respectively.

After scanning the undisturbed cores with X-ray CT (see below), we derived the bulk density of the cores gravimetrically. The water filled pore space was then calculated based on the measured water contents and the bulk density within the different plots. In addition, soil of these cores was used to measure the pH-value (in water).

Weather data (daily precipitation and temperature) are from <https://lter.kbs.msu.edu/datatables/12>.

X-ray CT

After the last sampling campaign in late August, one intact soil core (5 cm Ø, 5 cm height) was taken from 1 to 6 cm depth under the base of each static chamber (Fig. 1b). These

cores were subjected to X-ray CT shortly after collection. The soil cores were scanned using an X-ray microtomograph (X3000, North Star Imaging, Rogers, USA) at 75 kV and 470 μ A. Since the samples were scanned using a continuous subpixX mode, a resolution of 18.2 μ m could be achieved, although the respective energy settings resulted in a larger focal spot on the VarianL07 detector panel (size 1920 * 1536 pixels). During a scan with four subimages (2 rows and 2 columns), 2880 projections were acquired at 3 frames per second with an average of 2 frames. The 3D image reconstruction was performed with the eFX reconstruction software.

Image processing and analyses

The reconstructed images were cut into cubes of 1850x1850x2300 voxels in Fiji (V. 153n, Schindelin et al. 2012). This was done, to avoid analyzing disturbed regions at the core walls. Then the images were segmented into four classes, namely pores, soil matrix, POM and roots (Fig. 1c). For this, we used a random forest classifier trained in ILASTIK (Berg et al. 2019) to pore segments, soil matrix, and a class that includes roots and POM. To train the classifier, we used subvolumes of five randomly chosen images for annotation. The out-of-bag error was <0.01. We were not able to further compare image-based POM to POM conventionally analyzed, but a similar protocol was used by Schlüter et al. (2022) to show good agreement of image-based POM and conventionally analyzed POM. Moreover, visual expectation of the images showed no over-segmentation of POM particles, although under-segmentation could potentially happen for small POM particles due to our resolution of 18.2 μ m. Such small POM particles, however, seem to be distributed more evenly in the soil matrix (Schlüter et al. 2022) and therefore would not affect the analyzed distribution of POM. After segmenting all plant residues, we further differentiated between POM and roots in Fiji, in which objects of the mixed class were assigned to roots (Fig. 1d) only if they were connected to the outer boundary of the image and were larger than 10.000 voxels, i.e. approx. 0.06 cm³. For the latter, we used the “connected components labeling” and the “size opening” functions of the plugin MorphoLibJ (Version 1.4.3, Legland et al. 2016).

The anaerobic soil volume fraction, i.e., the volume fraction of air distance larger than a threshold (Fig. 1e), was calculated as written in Rohe et al. (2021) by computing the Euclidean Distance Transform for the pore image. In addition to computing the anaerobic soil volume fraction and the visible porosity (pores > 0.036 mm), we computed the Γ -indicator as a third metric to estimate oxygen supply. For this, the pore image was labelled using the connected component labelling from the plugin BoneJ2 plugin (V. 7.10, Domander et al. 2021). This image was used to calculate the

Γ -indicator, which is a metric of pore connectivity (Lucas et al. 2020).

To measure the volume of pores between 0.036 mm and 0.15 mm \varnothing , we used the local thickness method (Hildebrand and Rüeggsegger 1997) in Fiji. We refer to the volume of pores between 0.036 mm and 0.15 mm \varnothing by pores < 0.15 mm \varnothing and report their volume relative to the volume of the soil core. Additionally, the image of the Euclidean Distance Transform (Fig. 1e) was also used to calculate the mean distance of POM to macropores similar to Ortega-Ramírez et al. (2023). Note that one image of the switchgrass cores contained a massive volume of roots, as only the root sod was sampled (Fig. 1d). This sample was handled as an outlier, as the large root volume (>10 %) led to unreliable information on the soil matrix. It was also excluded from the bulk density estimation.

Statistical analysis

Effects of the plant treatment (maize vs. switchgrass vs. energy sorghum) on the studied flux data and isotopic characteristics as well soil structural properties derived from X-ray CT scans were investigated using linear mixed model approach implemented in the lme4-package (Bates et al. 2015) of R (V. 4.1.1). These models extend simple linear models to include the non-independent nature of our sample hierarchical structure, i.e. the different chambers within one plot. The random effects assigned consisted of the treatment plots, used as an error term for testing the plant treatment effect, and the flux chambers nested within the plots, used as an error term. Additionally, for the studied flux data and isotopic characteristics, the time point of sampling was added as a fixed factor to the model. Because on some dates only maize and energy sorghum were sampled, we constructed two models, the first including only dates with these two plant treatments, while the second contained only sampling campaigns of all three plant treatments. The assumptions of normality and homogeneity of variances were assessed using normal probability plots of the residuals and Levene's tests for equal variances, respectively. When the normality assumption was found to be violated, the data were logarithmically transformed; when the equal variance assumption was violated, the unequal variance models were fitted using the package 'nlme' in R, respectively.

To address our second research question concerning the evaluating soil structural properties as predictors of denitrification, we computed the correlation matrix of Pearson's correlation showing coefficients in R using the 'corrplot' package. In addition to the correlations including data from all sampling days, we computed these correlation matrixes for specific days for which all data (pore structure, N₂O, and soil chemistry) were available.

Due to the different management strategies of bioenergy crops we did not analyze the pore structural correlations with the total fluxes across the plant systems. For this, we computed plant treatment specific linear regressions of parameters derived from X-ray CT (anaerobic soil volume fraction, distance of POM to macropores, Pores $<150\mu\text{m}$) with the mean $\text{N}_2+\text{N}_2\text{O}$ emissions of the flux chambers. In addition, linear regression show the response of the fraction of bD and the pr to the anaerobic soil volume fraction and the distance of POM to macropores across the plant systems, where the fraction of bD as well as the pr were log scaled. Available NH_4^+ and NO_3^- were analyzed only in one sample per plot only, that is, no mixed effect model was necessary and we used an analysis of variance (ANOVA) in conjunction with Tukey's HSD test implemented in the 'agricolae' package (Mendiburu and Yaseen 2020).

Results

$\text{N}_2\text{O}+\text{N}_2$ fluxes

At the beginning of the season (early May), the perennial system switchgrass was wetter compared to maize and energy sorghum (Fig. 2b) systems. Fertilization of switchgrass during this time led to a peak in $\text{N}_2\text{O}+\text{N}_2$ emissions with fluxes $> 100 \text{ g N day}^{-1} \text{ ha}^{-1}$, with N_2O less than $25 \text{ g N day}^{-1} \text{ ha}^{-1}$ (Fig. 2c). Due to low precipitation (Fig. 2a), by late May WFPS had dropped substantially (Fig. 2b)

and N_2O emissions were barely detectable (Fig. 2c). The large rain event of mid-June led to high fluxes of $\text{N}_2\text{O}+\text{N}_2$ in all three systems, with both N_2O (approx. $75 \text{ g N day}^{-1} \text{ ha}^{-1}$) and $\text{N}_2\text{O}+\text{N}_2$ emissions significantly higher in energy sorghum compared to maize and switchgrass. Shortly after the first large rain event, the two annual crops were fertilized, and multiple heavy rains followed within two days, greatly increasing soil water contents. The $\text{N}_2\text{O}+\text{N}_2$ emissions after fertilization did not differ between energy sorghum and maize and were substantially lower than the emission peaks observed after the first rain event of 18 June. Seven days after this fertilization their $\text{N}_2\text{O}+\text{N}_2$ fluxes again increased substantially (approx. $100 \text{ g N day}^{-1} \text{ ha}^{-1}$), with a particularly large share of N_2O (approx. $50 \text{ g N day}^{-1} \text{ ha}^{-1}$). Interestingly, after the low June fluxes and despite the lack of fertilization, $\text{N}_2\text{O}+\text{N}_2$ emissions from switchgrass increased in early July and then again in late August, with a continuously low share of N_2O .

The mean $\text{N}_2\text{O}+\text{N}_2$ fluxes for the entire season did not differ significantly among the three crops (Table 1). Mean N_2O fluxes were significantly higher in energy sorghum ($18.6 \text{ g N day}^{-1} \text{ ha}^{-1}$) compared to maize ($14.6 \text{ g N day}^{-1} \text{ ha}^{-1}$), while numerically the lowest in switchgrass stands ($9.2 \text{ g N day}^{-1} \text{ ha}^{-1}$).

Soil NH_4^+ and NO_3^- concentrations did not significantly differ among the systems at any point during the season (Table S2) except in July when the soil of maize plots had significantly higher NO_3^- concentrations compared to energy sorghum and switchgrass.

Table 1 Mean values (\pm standard errors) of the main N_2O flux parameters and pore structural properties of the three bioenergy systems. Shown are measured N_2O fluxes, calculated $\text{N}_2\text{O}+\text{N}_2$ fluxes, the corresponding fraction of bacterial denitrification (bD), and the product ratio (pr) assuming a mixing of bacterial and fungal denitrification

in addition, also shown are the values of f_{bd} 2 and pr 2 calculated assuming a mixing of bD and nitrification (Ni). The Γ -indicator is the probability which describes the connectivity of the pore system. Different letters indicate significant differences between plant systems ($p<0.05$).

Treatment	Maize	Sorghum		Switchgrass		
N_2O flux [$\text{g N day}^{-1} \text{ ha}^{-1}$]	14.57	$\pm 2.33\text{a}$	18.64	$\pm 3.13\text{b}$	9.22	$\pm 2.61\text{a}$
$\text{N}_2\text{O} + \text{N}_2$ flux [$\text{g N day}^{-1} \text{ ha}^{-1}$]	29.64	$\pm 7.87\text{a}$	24.98	$\pm 6.75\text{a}$	31.70	$\pm 7.57\text{a}$
Fraction of bD [-]	0.79	$\pm 0.03\text{a}$	0.75	$\pm 0.05\text{a}$	0.95	$\pm 0.01\text{b}$
pr [-]	0.49	$\pm 0.03\text{b}$	0.49	$\pm 0.06\text{b}$	0.24	$\pm 0.01\text{a}$
Fraction of bD 2 [-]	0.86	$\pm 0.02\text{a}$	0.82	$\pm 0.04\text{a}$	0.96	$\pm 0.01\text{b}$
pr 2 [-]	0.27	$\pm 0.02\text{a}$	0.27	$\pm 0.02\text{a}$	0.19	$\pm 0.01\text{a}$
Macroporosity [% of total volume]	14.12	$\pm 1.17\text{a}$	13.18	$\pm 1.45\text{a}$	12.55	$\pm 0.80\text{a}$
Pores $<150 \mu\text{m}$ Ø [% of total volume]	5.77	$\pm 0.52\text{b}$	5.28	$\pm 1.05\text{ab}$	3.19	$\pm 0.45\text{a}$
POM [% of total volume]	0.95	$\pm 0.11\text{a}$	1.18	$\pm 0.16\text{a}$	1.21	$\pm 0.19\text{a}$
Root [% of total volume]	0.18	$\pm 0.01\text{a}$	0.21	$\pm 0.06\text{a}$	1.38	$\pm 0.28\text{b}$
anaerobic soil volume fraction [% of total volume]	4.44	$\pm 1.21\text{a}$	7.19	$\pm 1.97\text{a}$	14.51	$\pm 2.63\text{b}$
Distance of POM to macropores [mm]	0.09	$\pm 0.01\text{a}$	0.11	$\pm 0.01\text{b}$	0.14	$\pm 0.01\text{b}$
Γ -indicator [-]	0.75	$\pm 0.04\text{a}$	0.77	$\pm 0.06\text{a}$	0.79	$\pm 0.04\text{a}$
Bulk density [g cm^{-3}]	1.54	$\pm 0.05\text{a}$	1.56	$\pm 0.05\text{a}$	1.48	$\pm 0.06\text{a}$
pH [-]	6.53	$\pm 0.43\text{a}$	6.32	$\pm 0.43\text{a}$	5.86	$\pm 0.16\text{a}$

Isotopic Characterization

On most dates when isotopic characterization was performed for all three cropping systems switchgrass had higher $\delta^{18}\text{O}_{\text{N}_2\text{O}}$, $\delta^{15}\text{N}_{\text{bulk}}$, and lower $\delta^{15}\text{N}_{\text{SP}}$ values compared to maize and energy sorghum (Fig. S1). Only in late August, the N_2O from switchgrass had significantly lower $\delta^{18}\text{O}$ values compared to the two other plants. Consequently, in the isotopic mapping of $\delta^{18}\text{O} / \delta^{15}\text{N}_{\text{SP}}$ the maize and energy sorghum data are distributed mainly in-between the fD-bD mixing line and the reduction line, while the switchgrass data are mostly clustered around the reduction line (Fig. 3). High fluxes were directly associated with a higher fraction of bD (Fig. S2), thus yellow to red points in Fig. 3 are found only close to the reduction line.

Reasoned summarized isotopic endmember values from Yu et al. (2020) enable us to differentiate between two potential mixing lines (bD-Ni and bD-fD) and thus we must select the appropriate mixing scenario (Lewicka-Szczebak et al. 2020). In this study, the pr and the fraction of bD are nearly identical for both mixing scenarios (Fig. 4, Fig. S3). This is because of the generally high fraction of bD especially in switchgrass. As most points lay far below the bD-fD mixing line and are distant from Ni, indicating the low importance of Ni, we focus our analysis on the results in Fig. 4, assuming a primary mixing of bD and fD. That said, the influence of Ni (Fig. S3) cannot be excluded for all points and later is discussed separately.

The calculated values of the fraction of bD and pr from Fig. 3 revealed a high importance of bD in switchgrass systems and a large share of N_2O 's being reduced to N_2 as compared to maize and energy sorghum systems (Table 1, Fig. 4). An exception was the late August sampling date, where the fraction bD in switchgrass became numerically

lower and the pr numerically higher than those in maize and energy sorghum. While throughout the season energy sorghum and maize did not differ from each other in terms of either the fraction of bD and pr, shortly after fertilization energy sorghum had a significantly lower bD relative contribution compared to maize (Fig. 4). If we assume the mixing of bD and Ni only (Fig. S3), this would suggest that the importance of Ni was higher in sorghum systems compared to maize that particular sampling event, while on all other days there was no difference between the two crops in the relative contributions of Ni and bD to N_2O production. Indeed, the corresponding points can be found above the bD-fD mixing line in the subplot of energy sorghum (Fig. 3).

Correlation with pore structural properties

We conducted a sensitivity test and correlated the volume fraction of varying minimum distances to pores with the $\text{N}_2\text{O} + \text{N}_2$ fluxes to derive the anaerobic soil volume fraction (Rohe et al. 2021). While there was no significant correlation for switchgrass throughout all distances, the two other plants had significant correlations for a range of minimum distances (Fig. S4). For computing the final anaerobic soil volume fraction, we used the distance >0.41 mm away from pores, for which the lowest mean p-value for the two annual plants was found.

pH-values, bulk density, macroporosity (percent of pores $>40 \mu\text{m} \varnothing$), Γ -indicator (connectivity of the pore system), and percent POM were not significantly different among the three systems (Table 1). Yet, switchgrass had significantly higher root volumes and anaerobic soil volume fraction compared to energy sorghum and maize. Furthermore, switchgrass decreased the $<150 \mu\text{m} \varnothing$ pores and increased the mean distance from POM to macropores.

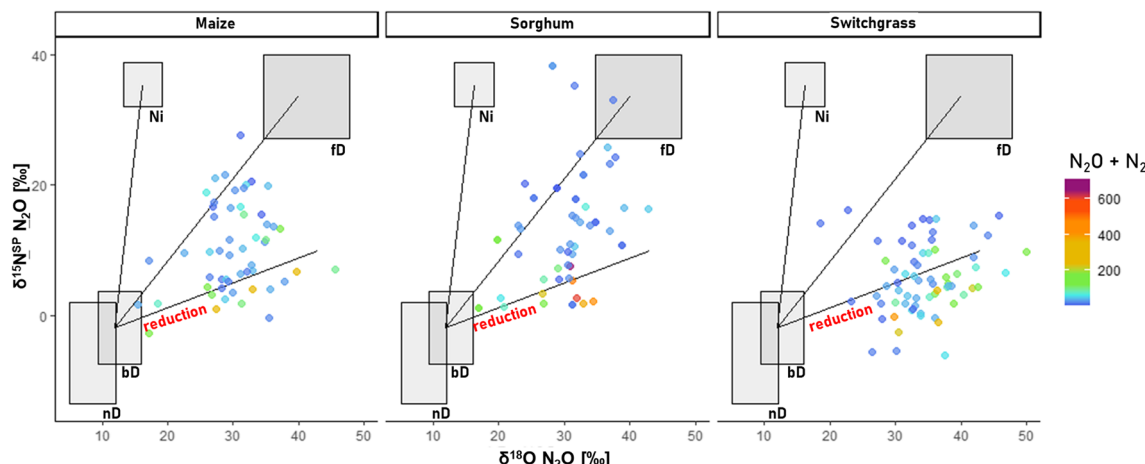
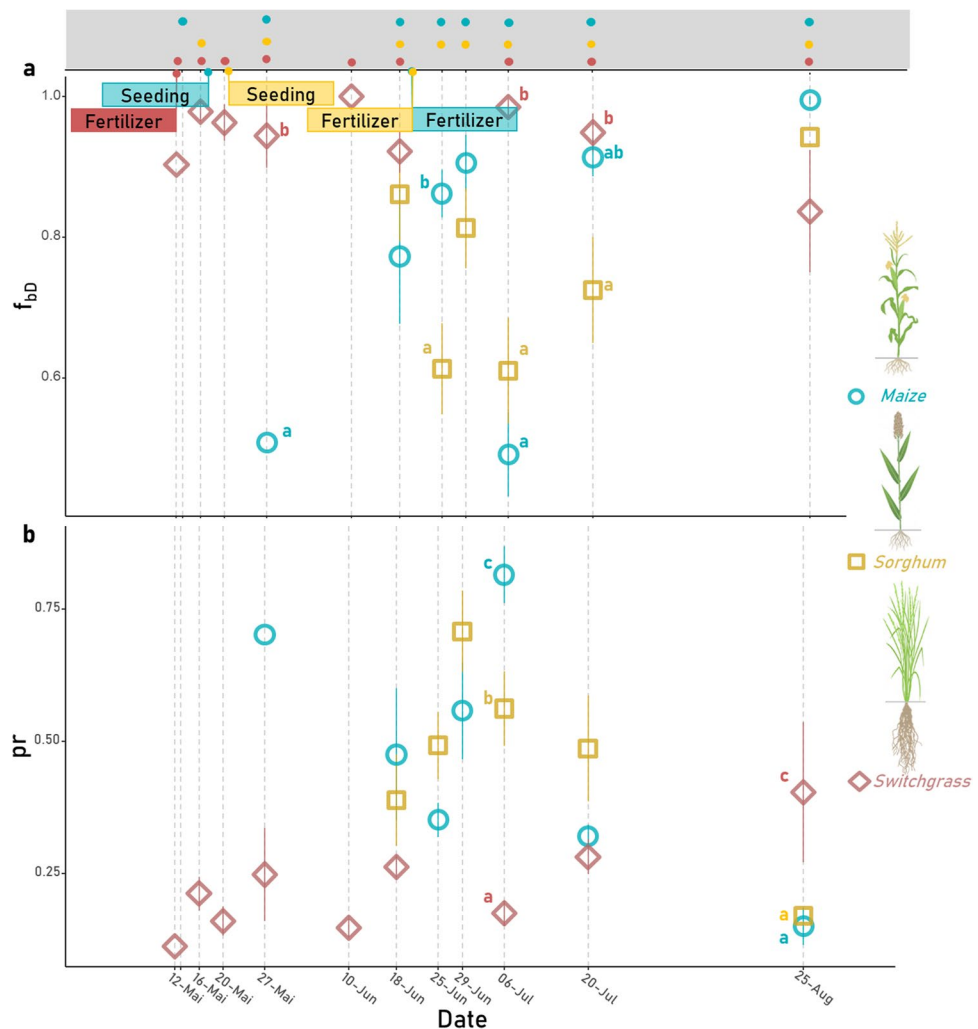


Fig. 3 Isotopic mapping for the three bioenergy crops. Squares show the end-members of Ni (nitrification), fD (fungal Denitrification), nD (nitrifier Denitrification) and bD (bacterial Denitrification)

Fig. 4 Fraction of N_2O originating from bacterial denitrification of total emitted N_2O (f_{bD}) and the denitrification product ratio (pr). The calculation assumes a mixing between bacterial denitrification and fungal denitrification.



Several of these properties were correlated with each other (Fig. S2a). The anaerobic soil volume fraction and the distance of POM to macropores were highly positively correlated, and both were negatively correlated to pores $<150 \mu\text{m} \varnothing$ and positively to the root volume.

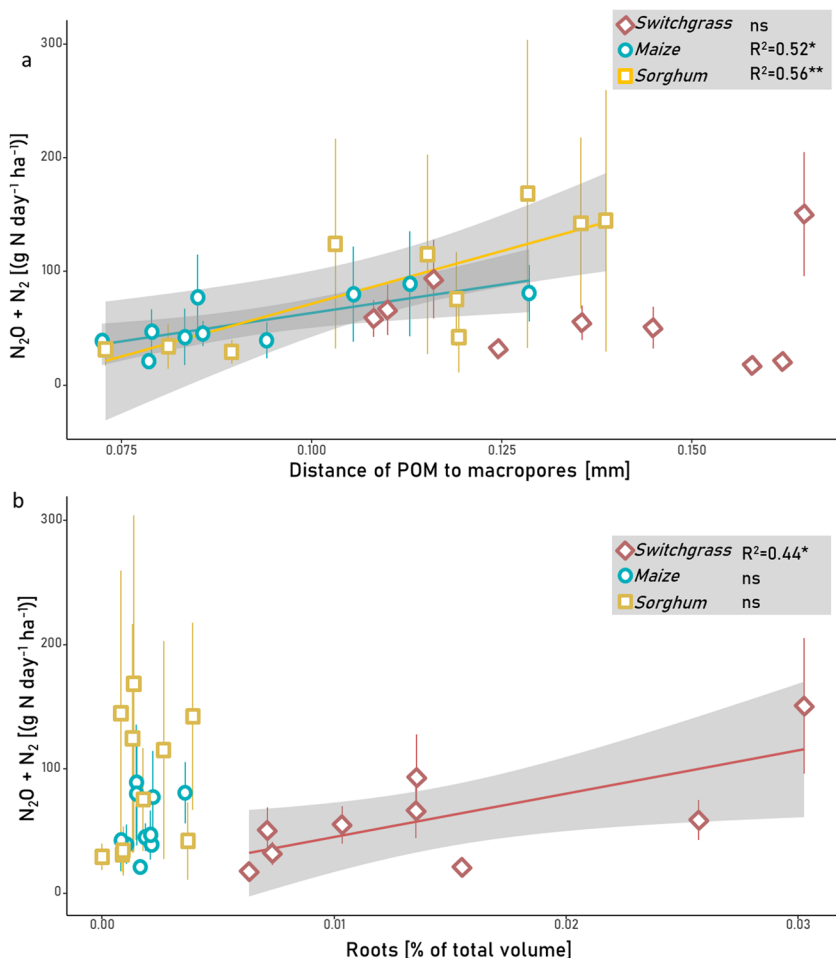
The distance of POM to macropores was positively correlated to $\text{N}_2\text{O} + \text{N}_2$ emissions in soils of maize and energy sorghum, but not in switchgrass (Fig. 5a). The same pattern was observed for the association between anaerobic soil volume fraction and $\text{N}_2\text{O} + \text{N}_2$ emissions (Fig. S5a). The abundance of $<150 \mu\text{m} \varnothing$ pores was related to $\text{N}_2\text{O} + \text{N}_2$ (negatively) only in sorghum soils (Fig. S5b). In addition, only in switchgrass was the root volume positively associated with the $\text{N}_2\text{O} + \text{N}_2$ emissions throughout the season (Fig. 5b).

Associations between $\text{N}_2\text{O} + \text{N}_2$ emissions and pore structure characteristics in the studied crops varied throughout the season (Fig. S2). For example, $\text{N}_2\text{O} + \text{N}_2$ emissions 7 days after fertilization (20th of May) were positively correlated to $< 150 \mu\text{m} \varnothing$ pores in switchgrass (Fig. S5c). The unexpectedly high $\text{N}_2\text{O} + \text{N}_2$ emissions in switchgrass soil

in late August was positively associated with the volume of roots observed within intact soil cores (Fig. S5d, $p < 0.1$), while not with other pore structural properties (not shown).

When examined across all three systems, there was a non-linear positive trend of the fraction of bd's increasing with increases in the anaerobic soil volume fraction (Fig. S6a) and the distance of POM to macropores (Fig. 6a). The fraction of bd was particularly low in soils of energy sorghum and maize when the soil anaerobic soil volume fraction was at its lowest and the distance from POM was at its highest, with bd fraction's as low as $<55\%$ in some energy sorghum plots. Note that this distance represents the mean of all POM within a given sample. The fraction of bd increased to $>90\%$ in switchgrass and plateaued after the distance of POM to macropores exceeded 0.1 mm. The trend was opposite for pr, which in energy sorghum and maize soils exceeded 60% at small anaerobic soil volume fractions and short distances to POM, and then decreased to $<50\%$ with increasing the distance of POM to macropores. Yet, pr was $<40\%$ in switchgrass soils across the entire range of observed distances of

Fig. 5 Relationship of the distance of POM to macropores (a) and roots (b) with $\text{N}_2\text{O} + \text{N}_2$ fluxes. Each point represents mean values of fluxes throughout the season for one static flux chamber. Stars indicate the significant association between the two parameters for the specific plant; $p < 0.05 = ^*$, $p < 0.01 = ^{**}$, ns = non-significant. Shadows show 95% confidence level interval for the predictions of the linear model.



POM to macropores. Note that the mean WFPS during the season did correlate with the total $\text{N}_2\text{O} + \text{N}_2$ emissions, but not with the fraction of bD and pr (Fig. S2a).

Discussion

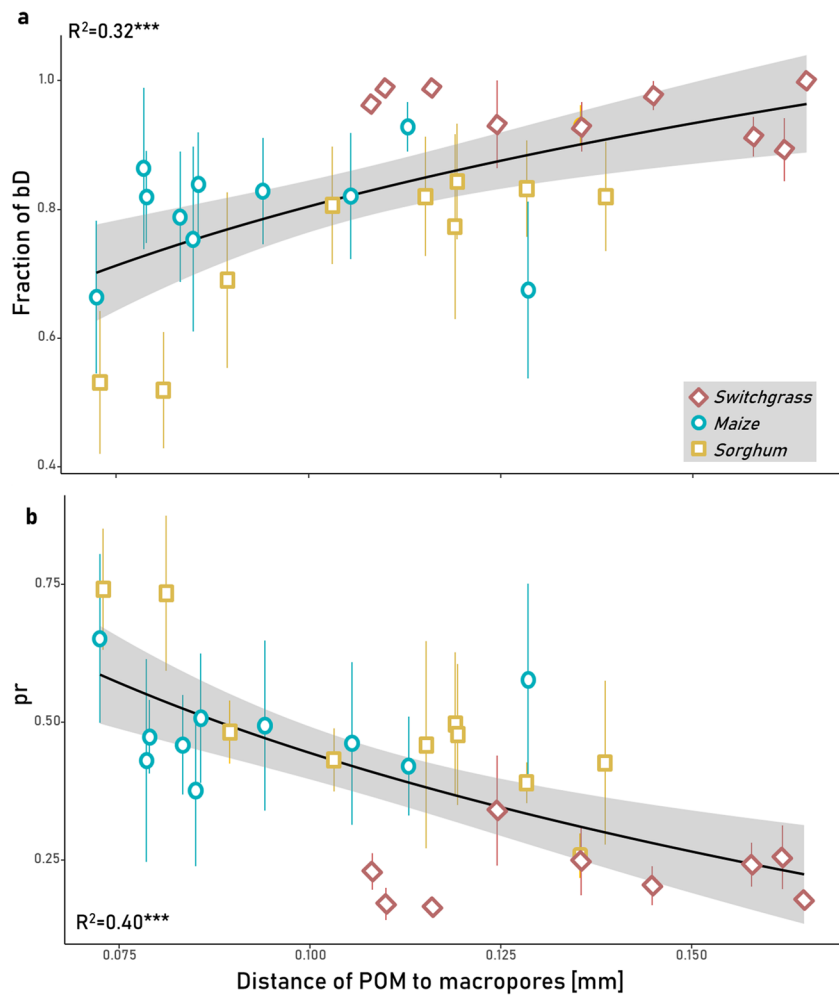
The effects of the pore structure on denitrification and N_2 production across bioenergy systems.

Our observations support the notion of high importance of bD in N_2O production, especially during events of high emissions (Fig. 3, Fig. 4a, Di Liang and Robertson 2021; Gao et al. 2023; Kravchenko et al. 2018; Ostrom et al. 2021). Furthermore, high anaerobic soil volume fractions and the distance of POM to macropores lead to a high amount of N_2O being reduced to N_2 (Fig. 6b,d). The reason for this could be that N_2O formed in the anaerobic soil volume fraction, e.g. at hotspots of occluded POM, can potentially be reduced to N_2 before it reaches the air-filled pore space (Braker and Conrad 2011; Rohe et al. 2021). As expected, high emissions of $\text{N}_2\text{O} + \text{N}_2$ corresponded to fertilizer

application dates and changing soil moisture (Fig. 2a). The change in pore structure, however, led to high N_2O emissions only in energy sorghum and maize, e.g. after fertilization (28th of June and 6th of July), where a relatively high denitrification pr [$\text{N}_2\text{O}/(\text{N}_2\text{O} + \text{N}_2)$] (Fig. 4b) resulted in N_2O fluxes $> 50 \text{ g N day}^{-1} \text{ ha}^{-1}$ (Fig. 2c). Thus, mean N_2O emissions increased in the order switchgrass < maize < energy sorghum (Table 1).

In rainfed areas of the US, bioenergy systems using sorghum were found to have comparable N_2O emissions to those using maize (Kent et al. 2020). Indeed, in our study the two systems behaved very similarly with 1) a peak after fertilization and 2) the reduced importance of bD one month after fertilization (Fig. 3a) as measured on the same fields two years before for maize (Fig. 2c, Ostrom et al. 2021), while the plots of switchgrass deviated from the others not only due to management strategies, e.g. different timing and amount of fertilization. Switchgrass was found to have lower N_2O emissions compared to maize (Tab. 1 and as shown before by Abraha et al. 2018 and Ostrom et al. 2021). The large anaerobic soil volume fractions in switchgrass, which were associated with a high fraction of bD and a low pr

Fig. 6 Influence of the distance of POM to macropores on (a) fraction of bacterial denitrification (bD) and the (b) denitrification product ratio (pr). Each point represents mean values of fluxes throughout the season for one static flux chamber. Stars indicate the significant association between the two parameters; $p < 0.05 = ^*$, $p < 0.01 = ^{**}$, ns = non-significant. Shadows show 95% confidence level interval for the predictions of the linear model.



(Tab. 1, Fig. S6), lead to relatively low N_2O emissions in switchgrass throughout the season (Fig. 2c). Even after the fertilization event in switchgrass (20th of May), N_2O emissions were low ($< 25 \text{ g N day}^{-1} \text{ ha}^{-1}$), while $\text{N}_2\text{O} + \text{N}_2$ emissions peaked at approx. $100 \text{ g N day}^{-1} \text{ ha}^{-1}$ (Fig. 2c). In such a system with high relative contribution of bD, gross N_2O consumption can exceed N_2O production, which can make denitrification a net N_2O sink (Philippot et al. 2011). Note that due to error propagation the calculation of N_2 emissions from isotopic mapping tend to be imprecise especially at low fluxes, where methodological uncertainties are highest. A comparison to the ^{15}N tracing technique applied to the field, however, showed that the mapping technique offers valid qualitative information about the N_2 emissions, which are due to the high atmospheric N_2 background rarely measured (Lewicka-Szczebak et al. 2020).

However, the distance threshold for anaerobic conditions was set to 0.41 mm, based on a sensitivity analyses before further evaluation (Fig. S4). This is more than double than that found by Kravchenko et al. (2018), but also about 1/10 of the 5 mm found by Rohe et al. (2021). The

latter's large distances, however, were related to repacked soil conditions, which can create completely different conditions with trapped gas pockets and reduced hotspots due to missing POM as compared to structured soil (Rohe et al. 2021). When, locally, the O_2 demand exceeds the O_2 supply, denitrification is favored (Rohe et al. 2021). Our results confirm former studies that show the capacity for X-ray CT to estimate the anaerobic soil volume fraction to describe O_2 availability (Kravchenko et al. 2018; Rabot et al. 2015; Rohe et al. 2021) and additionally to quantify local hotspots created by POM (Kim et al. 2020; Kravchenko et al. 2018; Ortega-Ramírez et al. 2023). These hotspots are microsites of high O_2 demand and unless connected to an air-filled macropore, anaerobic conditions develop that allow denitrification to occur. The anaerobic soil volume fraction and the distance of POM to macropores were highly correlated in our study (Fig. S2a), making both parameters equally good predictors of $\text{N}_2 + \text{N}_2\text{O}$ fluxes (Fig. 5a, Fig S5a) and of the activity of denitrifying bacteria (Fig. S6, Fig. S6a).

The highly negative correlation of pores $< 150 \mu\text{m}$ with the anaerobic soil volume fraction (Fig. 2a) is in

agreement with previous findings showing the importance of these pores to reduce the volume of anaerobic microsites (Kravchenko et al. 2018). Therefore, the $<150\text{ }\mu\text{m}$ Ø pores were negatively associated with $\text{N}_2\text{O}+\text{N}_2$ fluxes in energy sorghum, while no significant association was found in the two other plant systems (Fig. S5b). This is in contrast to the laboratory incubation experiments with fresh residue additions or roots of young recently terminated plants (Kim et al. 2020, 2022; Kravchenko et al. 2017). In these studies, N_2O emissions were enhanced by greater presence of $<150\text{ }\mu\text{m}$ pores Ø and an associated enhanced creation of hotspots due to the sponge effect of fresh decomposing plant and reveals that in the field the effect of the anaerobic soil volume fraction can counteract the sponge effect. The intact cores of our study contained residues of old as well as young roots as well as POM in a wide range of decomposition stages and thus provided a more realistic assessment of field processes.

The anaerobic soil volume fraction varies under changing water contents at the same time that local hotspots created through POM will change O_2 demand (Kravchenko et al. 2018; Rabot et al. 2015; Rohe et al. 2021; Schlüter et al. 2019). The relationship of bD with the anaerobic soil volume fraction and related structural properties derived from the cores taken in late August is therefore not on all days significant (Fig. S2). This was true, for instance, on 18 June, i.e. the day of the large rain event, when the anaerobic soil volume fraction was potentially much higher as estimated by our image analysis. On this day, however, Γ -indicator, i.e. the connectivity of the pore space, was negatively correlated with the $\text{N}_2\text{O} + \text{N}_2$ fluxes. The potential lower infiltration in plots with low connectivity increased the anaerobic soil volume fraction during the rain event and led, in combination with the higher amounts of available NO_3^- (Fig. S2d), to the burst of $\text{N}_2\text{O} + \text{N}_2$ especially in energy sorghum (Fig. 2c).

Despite these variabilities, our findings highlight the value of our method to connect N_2O production pathways during a crop season to microscale properties. In the future, pore scale modelling could be used to simulate the anaerobic soil volume fraction under contrasting conditions throughout the year and therefore improve the predictability of $\text{N}_2\text{O}+\text{N}_2$ emissions. To summarize, we have discovered a strong correlation between the anaerobic soil volume fraction and the distance of POM to macropores with the average fraction of bD in the bioenergy systems.

How the large roots system of the perennial switchgrass changes the N-cycle.

Switchgrass had lower N_2O emissions compared to maize (Tab. 1), making it a promising biofuel crop option for mitigating climate change due to its low greenhouse gas emissions (Monti et al. 2012). Switchgrass as a perennial crop builds its large root system over several years and then

maintains it, while most of the root system of sorghum and maize degrades shortly after harvest. The large volume of switchgrass roots create a pore structure dominated by large root-holding macropores at the expense of narrow macropores (Tab. 1), leading to larger anaerobic soil volume fraction and consequently high potential for bD (Fig. S6a, Fig. 4a). In addition, large volumes of POM generated from switchgrass massive root system serve as sources for denitrification (Fig. 6a). Thus, despite being supplied with only 1/3 of the N fertilizer, switchgrass showed numerically the highest $\text{N}_2\text{O}+\text{N}_2$ emissions compared to the annual systems (Tab. 1, Fig. 6a). Even though continuous measurements of the gas fluxes would be necessary to obtain unequivocal estimations for the entire season, our intermittently sampled data strongly suggest that switchgrass loses large amounts of the applied fertilizer N as N_2 . Higher $\text{N}_2\text{O}+\text{N}_2$ emissions from switchgrass is a novel finding given the lack of data in the literature for total denitrification.

Despite the high fraction of bD in switchgrass we found no significant association of the anaerobic soil volume fraction and the total $\text{N}_2+\text{N}_2\text{O}$ emitted. One reason could be that we only used 5 cm cores from the topsoil and therefore were not able to include potential subsoil properties guiding denitrification (Shcherbak and Robertson 2019). Another could be that the lower application of urea and the large root system in switchgrass systems enhance the role of the root system's affecting N-availability and consequently $\text{N}_2\text{O}+\text{N}_2$ production (Fig. 5b). Plant roots can modify the N balance in multiple ways; for example, the direct release of exudates can lead to priming effects, and the allocation of C to ectomycorrhizal fungi can increase the mineralization of org-N (Moreau et al. 2019). Such processes would release N in close proximity to switchgrass roots, i.e. the rhizosphere, which is potentially often compacted (Tab. 1) and would result in local anaerobic hotspots' driving complete denitrification (N_2O reduction to N_2). Note that the availability of such labile C form also drives denitrification (Baggs 2011; Groffman et al. 1988; Wrage et al. 2004). In addition, switchgrass is known to harness free living N-fixing bacteria (Roley et al. 2021), which could additionally fuel $\text{N}_2 + \text{N}_2\text{O}$ emissions.

After full aboveground development and pollination switchgrass undergoes senescence. During this period remobilization of plant N into roots prior to harvest occurs (Yang and Udvardi 2018). During the sampling of N_2O in late August, when the plant flowered, we found a decreasing importance of bD (Fig. 3a) and an increase in pr (Fig. 3b), while $\text{N}_2\text{O}+\text{N}_2$ fluxes were high (Fig. 2c). Interestingly, during this sampling date the root volume of switchgrass was positively correlated with total fluxes (Fig. S5d, $p < 0.1$). Considering that switchgrass roots, when grown in monoculture, are predominantly located in large macropores (Lucas et al. 2023), we can surmise that N_2O formed during the

decomposition of senescent roots with elevated N content (Yang et al. 2016) readily escapes to the atmosphere, leading to the observed increases in pr. From this, it follows that the N source for N_2O formation has shifted from the anaerobic soil volume fraction/matrix to the roots and their rhizodeposition, which however needs further investigation.

In summary, switchgrass with its massive root system stimulates denitrification both directly, by releasing labile N into the compacted rhizosphere, and indirectly, by forming large amounts of POM at large distances from macropores. This resulted in large N loses through $\text{N}_2\text{O}+\text{N}_2$ emissions.

The impact of BNI for the investigated sorghum variety

Our expectation was that 4 years of continuous cropping of energy sorghum with its potential for BNI (Subbarao et al. 2007) will lead to greater N_2O production through the denitrification pathway relative to the nitrification pathway by reducing gross nitrification as compared to maize (Nardi et al. 2022). Indeed, energy sorghum seem to be capable of reducing the amount of ammonia oxidizing bacteria under field conditions (Bozal-Leorri et al. 2023). However, during the study season, the denitrification-based N_2O gross production from the soil under energy sorghum was not greater than that from maize (Table 1). Moreover, on none of the sampling dates energy sorghum had significantly higher bD fraction than maize, while three days after fertilization (25th of June) the fraction of bD from sorghum soil was significantly lower compared to maize, suggesting a greater importance of nitrification (Fig. S3a) or fungal denitrification (Fig. 4a) there. The fertilization events with 28% urea-ammonium nitrate fertilizer and the rain event resulted in occasionally relatively high NH_4^+ -concentrations in the soils of both energy sorghum and maize systems (Tab. S2). The presence of NH_4^+ in the rhizosphere could have stimulated the exudation of BNIs (Subbarao et al. 2015). Note that the largest $\text{N}_2\text{O}+\text{N}_2$ emissions from energy sorghum occurred at the beginning of the season (Fig. 2c), while large effects on gross nitrification by BNIs requires root proliferation as found only later in the growing season. This is because sorgholeone, a major BNI component of sorghum, is hydrophobic and thus likely to be restricted to the rhizosphere (Dayan et al. 2010; Subbarao et al. 2013). But even hydrophilic-BNIs that can diffuse into the soil (Gao et al. 2022) would impact nitrification in a limited soil volume if the root system is still under development.

However, the release of BNIs by sorghum can be highly variable depending on genotype (Gao et al. 2022; Sarr et al. 2020; Subbarao et al. 2015; Tesfamariam et al. 2014). As there are, to the best of our knowledge, no detailed analyses of BNIs releases by the variety used in our study (TAM 17651) we cannot draw any conclusions about other sorghum

varieties. Thus, additional research with other varieties by using the isotopic mapping approach is needed to investigate the effect of BNI by sorghum on gross-denitrification on the field. In summary, the importance of bD was already high for all plants throughout the season (Fig. 4a), and we could not identify any effect of potential nitrification inhibition by sorghum, which would have led to even higher importance of bD.

Conclusions

For the first time, we were able to link microscale properties with $\text{N}_2\text{O}+\text{N}_2$ emissions and production pathways in an agricultural cropping season. We show that the anaerobic soil volume fraction and the distance of POM to macropores derived from X-ray CT are important factors for bacterial denitrification and can be used to cover local variability in $\text{N}_2\text{O}+\text{N}_2$ emissions in the field. The large changes in these microscale properties measured across and within the investigated plant systems highlight the effect of certain plant species on pore structure and their potential use to mitigate GHG emissions. Although our study reflects fluxes from only a single season, and a multi-year observation period would be needed to assess long-term effects of cropping histories and soil structural differences on $\text{N}_2\text{O}+\text{N}_2$ emissions in field settings, results nonetheless demonstrate the feasibility and usefulness of $\text{N}_2\text{O}+\text{N}_2$ monitoring in combination with pore structural analysis in the field. Results also show the value of a future research focus on root traits' leading to changes in pore structure and the distribution of POM, with the potential to reduce N loses by $\text{N}_2\text{O}+\text{N}_2$. Finally, our data questions the importance of BNI for the investigated sorghum variety, as we found no evidence for reduced gross nitrification.

Supplementary Information The online version contains supplementary material available at <https://doi.org/10.1007/s00374-023-01761-1>.

Acknowledgments We thank Stacey Vanderwulp and Kevin Kahrmark for their assistance with field flux chamber installation and sample collection. We thank Maxwell Oerther for his help during soil sampling and processing, Michelle Quigley for her support during the X-ray CT scans. The authors gratefully acknowledge the help of Hasand Gandhi and Samuel DeCamp with the isotopic analysis. We thank the anonymous reviewers for their suggestions, which greatly improved the manuscript.

This research was funded in part by the Great Lakes Bioenergy Research Center, U.S. Department of Energy, Office of Science, Office of Biological and Environmental Research under Award Number DE-SC0018409, by the NSF LTER Program (DEB 1027253) at the Kellogg Biological Station, and by Michigan State University AgBioResearch. The Great Lakes Bioenergy Research Center provided the open access funding.

Declarations

Competing interests The authors declare no competing interests.

Open Access This article is licensed under a Creative Commons Attribution 4.0 International License, which permits use, sharing, adaptation, distribution and reproduction in any medium or format, as long as you give appropriate credit to the original author(s) and the source, provide a link to the Creative Commons licence, and indicate if changes were made. The images or other third party material in this article are included in the article's Creative Commons licence, unless indicated otherwise in a credit line to the material. If material is not included in the article's Creative Commons licence and your intended use is not permitted by statutory regulation or exceeds the permitted use, you will need to obtain permission directly from the copyright holder. To view a copy of this licence, visit <http://creativecommons.org/licenses/by/4.0/>.

References

Abraha M, Gelfand I, Hamilton SK, Chen J, Robertson GP (2018) Legacy effects of land use on soil nitrous oxide emissions in annual crop and perennial grassland ecosystems. *Ecol Appl* 28:1362–1369. <https://doi.org/10.1002/eaap.1745>

Andersen AJ, Petersen SO (2009) Effects of C and N availability and soil-water potential interactions on N_2O evolution and PLFA composition. *Soil Biol Biochem* 41:1726–1733. <https://doi.org/10.1016/j.soilbio.2009.06.001>

Bacq-Labreuil A, Crawford J, Mooney SJ, Neal AL, Ritz K (2019) Cover crop species have contrasting influence upon soil structural genesis and microbial community phenotype. *Sci Rep* 9:7473. <https://doi.org/10.1038/s41598-019-43937-6>

Baggs EM (2011) Soil microbial sources of nitrous oxide: recent advances in knowledge, emerging challenges and future direction. *Curr Opin Environ Sustain* 3:321–327. <https://doi.org/10.1016/j.cosust.2011.08.011>

Balaine N, Clough TJ, Beare MH, Thomas SM, Meenken ED, Ross JG (2013) Changes in Relative Gas Diffusivity Explain Soil Nitrous Oxide Flux Dynamics. *Soil Sci Soc Am J* 77:1496–1505. <https://doi.org/10.2136/sssaj2013.04.0141>

Bates D, Mächler M, Bolker B, Walker S (2015) Fitting Linear Mixed-Effects Models Using lme4. *J Stat Softw* 67:1–48. <https://doi.org/10.18637/jss.v067.i01>

Berendsen RL, Pieterse CM, Bakker PA (2012) The rhizosphere microbiome and plant health. *Trends in Plant Sci* 17:478–486. <https://doi.org/10.1016/j.tplants.2012.04.001>

Berg S, Kutra D, Kroeger T, Straehle CN, Kausler BX, Haubold C, Schiegg M, Ales J, Beier T, Rudy M, Eren K, Cervantes JI, Xu B, Beuttenmueller F, Wolny A, Zhang C, Koethe U, Hamprecht FA, Kreshuk A (2019) ilastik: interactive machine learning for (bio)image analysis. *Nat Methods* 16:1226–1232. <https://doi.org/10.1038/s41592-019-0582-9>

Bodner G, Leitner D, Kaul H-P (2014) Coarse and fine root plants affect pore size distributions differently. *Plant Soil* 380:133–151. <https://doi.org/10.1007/s11104-014-2079-8>

Bollmann A, Conrad R (1998) Influence of O_2 availability on NO and N_2O release by nitrification and denitrification in soils. *Glob Chang Biol* 4:387–396. <https://doi.org/10.1046/j.1365-2486.1998.00161.x>

Bozal-Leorri A, Corrochano-Monsalve M, Arregui LM, Aparicio-Tejo PM, González-Murua C (2023) Evaluation of a crop rotation with biological inhibition potential to avoid N_2O emissions in comparison with synthetic nitrification inhibition. *J Environ Sci (China)* 127:222–233. <https://doi.org/10.1016/j.jes.2022.04.035>

Braker G, Conrad R (2011) Diversity, structure, and size of N_2O -producing microbial communities in soils--what matters for their functioning? *Adv Appl Microbiol* 75:33–70. <https://doi.org/10.1016/B978-0-12-387046-9.00002-5>

Butterbach-Bahl K, Dannenmann M (2011) Denitrification and associated soil N_2O emissions due to agricultural activities in a changing climate. *Curr Opin Environ Sustain* 3:389–395. <https://doi.org/10.1016/j.cosust.2011.08.004>

Butterbach-Bahl K, Baggs EM, Dannenmann M, Kiese R, Zechmeister-Boltenstern S (2013) Nitrous oxide emissions from soils: how well do we understand the processes and their controls? *Philos Trans R Soc Lond B Biol Sci* 368:20130122. <https://doi.org/10.1098/rstb.2013.0122>

Chen H, Williams D, Walker JT, Shi W (2016) Probing the biological sources of soil N_2O emissions by quantum cascade laser-based ^{15}N isotopocule analysis. *Soil Biol Biochem* 100:175–181. <https://doi.org/10.1016/j.soilbio.2016.06.015>

Dayan FE, Rimando AM, Pan Z, Baerson SR, Gimsing AL, Duke SO (2010) Sorgoleone. *Phytochemistry* 71:1032–1039. <https://doi.org/10.1016/j.phytochem.2010.03.011>

de Mendiburu F, Yaseen M (2020) agricolae: Statistical Procedures for Agricultural Research. R package version 1.4.0, <https://myaseen208.github.io/agricolae/> <https://cran.r-project.org/package=agricolae>

Di L, Robertson GP (2021) Nitrification is a minor source of nitrous oxide (N_2O) in an agricultural landscape and declines with increasing management intensity. *Glob Chang Biol* 27:5599–5613. <https://doi.org/10.1111/gcb.15833>

Doane TA, Horwath WR (2003) Spectrophotometric determination of nitrate with a single reagent. *Anal Lett* 36:2713–2722. <https://doi.org/10.1081/AL-120024647>

Domander R, Felder AA, Doube M (2021) BoneJ2 - refactoring established research software. *Wellcome Open Res* 6:37. 10.12688/wellcomeopenres.16619.2

Gao X, Uno K, Sarr PS, Yoshihashi T, Zhu Y, Subbarao GV (2022) High-sorgoleone producing sorghum genetic stocks suppress soil nitrification and N_2O emissions better than low-sorgoleone producing genetic stocks. *Plant Soil* 477:793–805. <https://doi.org/10.1007/s11104-022-05474-6>

Gao N, Zhang F, Bo Q, An T, Gao J, Wei X, Yue S, Shen Y, Li S (2023) Microbial and isotopomer analysis of N_2O production pathways in a calcareous film-mulched farmland. *Biol Fertil Soils* 59:407–422. <https://doi.org/10.1007/s00374-023-01711-x>

Groffman PM, Tiedje JM, Robertson GP, Christensen S (1988) Denitrification at different temporal and geographical scales: proximal and distal controls. In: Wilson JR (ed) Advances in nitrogen cycling in agricultural ecosystems: Proceedings of a Symposium on Advances in Nitrogen Cycling in Agricultural Ecosystems, held in Brisbane, Australia, 11–15 May 1987. C.A.B. International, Oxon, pp 174–192

Hildebrand T, Rüegsegger P (1997) A new method for the model-independent assessment of thickness in three-dimensional images. *J Microsc* 185:67–75. <https://doi.org/10.1046/j.1365-2818.1997.1340694.x>

Hinsinger P, Bengough AG, Vetterlein D, Young IM (2009) Rhizosphere: biophysics, biogeochemistry and ecological relevance. *Plant Soil* 321:117–152. <https://doi.org/10.1007/s11104-008-9885-9>

Jones DL, Nguyen C, Finlay RD (2009) Carbon flow in the rhizosphere: carbon trading at the soil–root interface. *Plant Soil* 321:5–33. <https://doi.org/10.1007/s11104-009-9925-0>

Kent J, Hartman MD, Lee DK, Hudiburg T (2020) Simulated biomass sorghum GHG reduction potential is similar to maize. *Environ Sci Technol* 54:12456–12466. <https://doi.org/10.1021/acs.est.0c01676>

Kim K, Guber A, Rivers M, Kravchenko A (2020) Contribution of decomposing plant roots to N₂O emissions by water absorption. *Geoderma* 375:114506. <https://doi.org/10.1016/j.geoderma.2020.114506>

Kim K, Kutlu T, Kravchenko A, Guber A (2021) Dynamics of N₂O in vicinity of plant residues: a microsensor approach. *Plant Soil* 462:331–347. <https://doi.org/10.1007/s11104-021-04871-7>

Kim K, Gil J, Ostrom NE, Gandhi H, Oerther MS, Kuzyakov Y, Guber AK, Kravchenko AN (2022) Soil pore architecture and rhizosphere legacy define N₂O production in root detritusphere. *Soil Biol Biochem* 166:108565. <https://doi.org/10.1016/j.soilbio.2022.108565>

Kravchenko AN, Toosi ER, Guber AK, Ostrom NE, Yu J, Azeem K, Rivers ML, Robertson GP (2017) Hotspots of soil N₂O emission enhanced through water absorption by plant residue. *Nature Geosci* 10:496–500. <https://doi.org/10.1038/ngeo2963>

Kravchenko AN, Guber AK, Quigley MY, Koestel J, Gandhi H, Ostrom NE (2018) X-ray computed tomography to predict soil N₂O production via bacterial denitrification and N₂O emission in contrasting bioenergy cropping systems. *GCB Bioenergy* 10:894–909. <https://doi.org/10.1111/gcbb.12552>

Kravchenko AN, Guber AK, Razavi BS, Koestel J, Quigley MY, Robertson GP, Kuzyakov Y (2019) Microbial spatial footprint as a driver of soil carbon stabilization. *Nat Commun* 10:3121. <https://doi.org/10.1038/s41467-019-11057-4>

Kravchenko AN, Richardson JA, Lee JH, Guber AK (2022) Distribution of Mn Oxidation States in Grassland Soils and Their Relationships with Soil Pores. 56:16462–16472 *Environ Sci Technol*. <https://doi.org/10.1021/acs.est.2c05403>

Legland D, Arganda-Carreras I, Andrey P (2016) MorphoLibJ: integrated library and plugins for mathematical morphology with ImageJ. *Bioinformatics* 32:3532–3534. <https://doi.org/10.1093/bioinformatics/btw413>

Lewicka-Szczebak D (2018) Mapping approach model after Lewicka-Szczebak et al. (2017) - detailed description of calculation procedures. 10.13140/RG.2.2.17478.52804

Lewicka-Szczebak D, Augustin J, Giesemann A, Well R (2017) Quantifying N₂O reduction to N₂ based on N₂O isotopocules – validation with independent methods (helium incubation and ¹⁵N gas flux method). *Biogeosciences* 14:711–732. <https://doi.org/10.5194/bg-14-711-2017>

Lewicka-Szczebak D, Lewicki MP, Well R (2020) N₂O isotope approaches for source partitioning of N₂O production and estimation of N₂O reduction – validation with the ¹⁵N gas-flux method in laboratory and field studies. *Biogeosciences* 17:5513–5537. <https://doi.org/10.5194/bg-17-5513-2020>

Li Y, Zhang Y, Chapman SJ, Yao H (2021) Biological nitrification inhibition by sorghum root exudates impacts ammonia-oxidizing bacteria but not ammonia-oxidizing archaea. *Biol Fertil Soils* 57:399–407. <https://doi.org/10.1007/s00374-020-01538-w>

Lucas M, Santiago JP, Chen J, Guber A, Kravchenko A (2023) The soil pore structure encountered by roots affects plant-derived carbon inputs and fate. *New Phytol*. <https://doi.org/10.1111/nph.19159>

Lucas M, Schlüter S, Vogel H-J, Vetterlein D (2019) Roots compact the surrounding soil depending on the structures they encounter. *Sci Rep* 9:16236. <https://doi.org/10.1038/s41598-019-52665-w>

Lucas M, Vetterlein D, Vogel H-J, Schlüter S (2020) Revealing pore connectivity across scales and resolutions with X-ray CT. *Eur J Soil Sci*. <https://doi.org/10.1111/ejss.12961>

Lucas M, Nguyen LTT, Guber A, Kravchenko AN (2022) Cover crop influence on pore size distribution and biopore dynamics: Enumerating root and soil faunal effects. *Front Plant Sci* 13:928569. <https://doi.org/10.3389/fpls.2022.928569>

McGill BM, Hamilton SK, Millar N, Robertson GP (2018) The greenhouse gas cost of agricultural intensification with groundwater irrigation in a Midwest U.S. row cropping system. *Glob Chang Biol* 24:5948–5960. <https://doi.org/10.1111/gcb.14472>

McSwiney CP, Robertson GP (2005) Nonlinear response of N₂O flux to incremental fertilizer addition in a continuous maize (*Zea mays* L.) cropping system. *Glob Chang Biol* 11:1712–1719. <https://doi.org/10.1111/j.1365-2486.2005.01040.x>

Monti A, Barbanti L, Zatta A, Zegada-Lizárrazu W (2012) The contribution of switchgrass in reducing GHG emissions. *Glob. Change Biol. Bioenergy* 4:420–434. <https://doi.org/10.1111/j.1757-1707.2011.01142.x>

Moreau D, Bardgett RD, Finlay RD, Jones DL, Philippot L (2019) A plant perspective on nitrogen cycling in the rhizosphere. *Funct Ecol* 33:540–552. <https://doi.org/10.1111/1365-2435.13303>

Müller C, Laughlin RJ, Spott O, Rütting T (2014) Quantification of N₂O emission pathways via a ¹⁵N tracing model. *Soil Biol Biochem* 72:44–54. <https://doi.org/10.1016/j.soilbio.2014.01.013>

Nardi P, Müller C, Pietramellara G, Subbarao GV, Nannipieri P (2022) Recommendations about soil Biological Nitrification Inhibition (BNI) studies. *Biol Fertil Soils* 58:613–615. <https://doi.org/10.1007/s00374-022-01645-w>

Oates LG, Duncan DS, Gelfand I, Millar N, Robertson GP, Jackson RD (2016) Nitrous oxide emissions during establishment of eight alternative cellulosic bioenergy cropping systems in the North Central United States. *GCB Bioenergy* 8:539–549. <https://doi.org/10.1111/gcbb.12268>

Ortega-Ramírez P, Pot V, Laville P, Schlüter S, Amor-Quiroz DA, Hadjar D, Mazurier A, Lacoste M, Caurel C, Pouteau V, Chenu C, Basile-Doelsch I, Henault C, Garnier P (2023) Pore distances of particulate organic matter predict N₂O emissions from intact soil at moist conditions. *Geoderma* 429:116224. <https://doi.org/10.1016/j.geoderma.2022.116224>

Ostrom NE, Gandhi H, Coplen TB, Toyoda S, Böhlke JK, Brand WA, Casciotti KL, Dyckmans J, Giesemann A, Mohn J, Well R, Yu L, Yoshida N (2018) Preliminary assessment of stable nitrogen and oxygen isotopic composition of USGS51 and USGS52 nitrous oxide reference gases and perspectives on calibration needs. *Rapid Commun Mass Spectrom* 32:1207–1214. <https://doi.org/10.1002/rcm.8157>

Ostrom PH, DeCamp S, Gandhi H, Haslun J, Ostrom NE (2021) The influence of tillage and fertilizer on the flux and source of nitrous oxide with reference to atmospheric variation using laser spectroscopy. *Biogeochemistry*. <https://doi.org/10.1007/s10533-020-00742-y>

Philippot L, Hallin S, Börjesson G, Baggs EM (2009) Biochemical cycling in the rhizosphere having an impact on global change. *Plant Soil* 321:61–81. <https://doi.org/10.1007/s11104-008-9796-9>

Philippot L, Andert J, Jones CM, Bru D, Hallin S (2011) Importance of denitrifiers lacking the genes encoding the nitrous oxide reductase for N₂O emissions from soil. *Glob Chang Biol* 17:1497–1504

Qin Z, Zhuang Q, Zhu X (2015) Carbon and nitrogen dynamics in bioenergy ecosystems: 2. Potential greenhouse gas emissions and global warming intensity in the conterminous United States. *GCB Bioenergy* 7:25–39. <https://doi.org/10.1111/gcbb.12106>

Rabot E, Lacoste M, Hénault C, Cousin I (2015) Using X-ray Computed Tomography to Describe the Dynamics of Nitrous Oxide Emissions during Soil Drying. *Vadose Zone Journal* 14:vzj2014.12.0177. <https://doi.org/10.2136/vzj2014.12.0177>

Ravishankara AR, Daniel JS, Portmann RW (2009) Nitrous oxide (N₂O): the dominant ozone-depleting substance emitted in the 21st century. *Science* 326:123–125. <https://doi.org/10.1126/science.1176985>

Robertson GP, Groffman PM (2015) Nitrogen Transformations. In: Paul EA (ed) *Soil Microbiology*. Elsevier, Ecology and Biochemistry (Fourth Edition), pp 421–446

Robertson GP, Hamilton SK (2015) Long-term ecological research in agricultural landscapes at the Kellogg Biological Station LTER

site: conceptual and experimental framework. In: Hamilton SK, Doll JE, Robertson GP (Eds) *The Ecology of Agricultural Landscapes: Long-Term Research on the Path to Sustainability*. Oxford, UK, pp 1–32

Rohe L, Apelt B, Vogel H-J, Well R, Wu G-M, Schlüter S (2021) Denitrification in soil as a function of oxygen availability at the microscale. *Biogeosciences* 18:1185–1201. <https://doi.org/10.5194/bg-18-1185-2021>

Roley SS, Ulbrich TC, Robertson GP (2021) Nitrogen Fixation and Resorption Efficiency Differences Among Twelve Upland and Lowland Switchgrass Cultivars. *Phytobiomes J* 5:97–107. <https://doi.org/10.1094/PBIOMES-11-19-0064-FI>

Sarr PS, Ando Y, Nakamura S, Deshpande S, Subbarao GV (2020) Sorgoleone release from sorghum roots shapes the composition of nitrifying populations, total bacteria, and archaea and determines the level of nitrification. *Biol Fertil Soils* 56:145–166. <https://doi.org/10.1007/s00374-019-01405-3>

Schindelin J, Arganda-Carreras I, Frise E, Kaynig V, Longair M, Pietzsch T, Preibisch S, Rueden C, Saalfeld S, Schmid B, Tinevez J-Y, White DJ, Hartenstein V, Eliceiri K, Tomancak P, Cardona A (2012) Fiji: an open-source platform for biological-image analysis. *Nat Methods* 9:676–682. <https://doi.org/10.1038/nmeth.2019>

Schlüter S, Henjes S, Zawallich J, Bergaust L, Horn M, Ippisch O, Vogel H-J, Dörsch P (2018) Denitrification in Soil Aggregate Analogues—Effect of Aggregate Size and Oxygen Diffusion. *Front. Environ. Sci.* 6. <https://doi.org/10.3389/fenvs.2018.00017>

Schlüter S, Zawallich J, Vogel H-J, Dörsch P (2019) Physical constraints for respiration in microbial hotspots in soil and their importance for denitrification. *Biogeosciences* 16:3665–3678. <https://doi.org/10.5194/bg-16-3665-2019>

Schlüter S, Leuther F, Albrecht L, Hoeschen C, Kilian R, Surey R, Mikutta R, Kaiser K, Mueller CW, Vogel H-J (2022) Microscale carbon distribution around pores and particulate organic matter varies with soil moisture regime. *Nat Commun* 13:2098. <https://doi.org/10.1038/s41467-022-29605-w>

Shcherbak I, Robertson GP (2019) Nitrous Oxide (N_2O) Emissions from Subsurface Soils of Agricultural Ecosystems. *Ecosystems* 22:1650–1663. <https://doi.org/10.1007/s10021-019-00363-z>

Sinsabaugh R, Reynolds H, Long T (2000) Rapid assay for amidohydrolase (urease) activity in environmental samples. *Soil Biol Biochem* 32:2095–2097. [https://doi.org/10.1016/S0038-0717\(00\)00102-4](https://doi.org/10.1016/S0038-0717(00)00102-4)

Stehfest E, Bouwman L (2006) N_2O and NO emission from agricultural fields and soils under natural vegetation: summarizing available measurement data and modeling of global annual emissions. *Nutr Cycl Agroecosyst* 74:207–228. <https://doi.org/10.1007/s10705-006-9000-7>

Subbarao GV, Rondon M, Ito O, Ishikawa T, Rao IM, Nakahara K, Lascano C, Berry WL (2007) Biological nitrification inhibition (BNI)—is it a widespread phenomenon? *Plant Soil* 294:5–18. <https://doi.org/10.1007/s11104-006-9159-3>

Subbarao GV, Nakahara K, Ishikawa T, Ono H, Yoshida M, Yoshihashi T, Zhu Y, Zakir HAKM, Deshpande SP, Hash CT, Sahrawat KL (2013) Biological nitrification inhibition (BNI) activity in sorghum and its characterization. *Plant Soil* 366:243–259. <https://doi.org/10.1007/s11104-012-1419-9>

Subbarao GV, Yoshihashi T, Worthington M, Nakahara K, Ando Y, Sahrawat KL, Rao IM, Lata J-C, Kishii M, Braun H-J (2015) Suppression of soil nitrification by plants. *Plant Sci* 233:155–164. <https://doi.org/10.1016/j.plantsci.2015.01.012>

Sutka RL, Ostrom NE, Ostrom PH, Gandhi H, Breznak JA (2003) Nitrogen isotopomer site preference of N_2O produced by *Nitrosomonas europaea* and *Methylococcus capsulatus* Bath. *Rapid Commun Mass Spectrom* 17:738–745. <https://doi.org/10.1002/rcm.968>

Syakila A, Kroese C (2011) The global nitrous oxide budget revisited. *GHG Measure Manage* 1(1):17–26. <https://doi.org/10.3763/ghgmm.2010.0007>

Tesfamariam T, Yoshinaga H, Deshpande SP, Srinivasa Rao P, Sahrawat KL, Ando Y, Nakahara K, Hash CT, Subbarao GV (2014) Biological nitrification inhibition in sorghum: the role of sorgoleone production. *Plant Soil* 379:325–335. <https://doi.org/10.1007/s11104-014-2075-z>

Tian H, Xu R, Canadell JG, Thompson RL, Winiwarter W, Suntharalingam P, Davidson EA, Ciais P, Jackson RB, Janssens-Maenhout G, Prather MJ, Regnier P, Pan N, Pan S, Peters GP, Shi H, Tubiello FN, Zaehele S, Zhou F et al (2020) A comprehensive quantification of global nitrous oxide sources and sinks. *Nature* 586:248–256. <https://doi.org/10.1038/s41586-020-2780-0>

Walter K, Don A, Flessa H (2015) Net N_2O and CH_4 soil fluxes of annual and perennial bioenergy crops in two central German regions. *Biomass Bioenergy* 81:556–567. <https://doi.org/10.1016/j.biombioe.2015.08.011>

Wightman JL, Duxbury JM, Woodbury PB (2015) Land Quality and Management Practices Strongly Affect Greenhouse Gas Emissions of Bioenergy Feedstocks. *Bioenerg. Res.* 8:1681–1690. <https://doi.org/10.1007/s12155-015-9620-3>

Wrage N, Velthof G, van Beusichem M, Oenema O (2001) Role of nitrifier denitrification in the production of nitrous oxide. *Soil Biol Biochem* 33:1723–1732. [https://doi.org/10.1016/S0038-0717\(01\)00096-7](https://doi.org/10.1016/S0038-0717(01)00096-7)

Wrage N, Lauf J, Del Prado A, Pinto M, Pietrzak S, Yamulki S, Oenema O, Gebauer G (2004) Distinguishing sources of N_2O in European grasslands by stable isotope analysis. *Rapid Commun Mass Spectrom* 18:1201–1207. <https://doi.org/10.1002/rcm.1461>

Yang J, Udvardi M (2018) Senescence and nitrogen use efficiency in perennial grasses for forage and biofuel production. *J Exp Bot* 69:855–865. <https://doi.org/10.1093/jxb/erx241>

Yang J, Worley E, Ma Q, Li J, Torres-Jerez I, Li G, Zhao PX, Xu Y, Tang Y, Udvardi M (2016) Nitrogen remobilization and conservation, and underlying senescence-associated gene expression in the perennial switchgrass *Panicum virgatum*. *New Phytol* 211:75–89. <https://doi.org/10.1111/nph.13898>

Yu L, Harris E, Lewicka-Szczebak D, Barthel M, Blomberg MRA, Harris SJ, Johnson MS, Lehmann MF, Liisberg J, Müller C, Ostrom NE, Six J, Toyoda S, Yoshida N, Mohn J (2020) What can we learn from N_2O isotope data? - Analytics, processes and modelling. *Rapid Commun Mass Spectrom* 34:e8858. <https://doi.org/10.1002/rcm.8858>

Yunusa IAM, Newton PJ (2003) Plants for amelioration of subsoil constraints and hydrological control: the primer-plant concept. *Plant Soil* 257:261–281. <https://doi.org/10.1023/A:1027381329549>

Publisher's note Springer Nature remains neutral with regard to jurisdictional claims in published maps and institutional affiliations.